Modeling and control of ibuprofen crystal growth and size distribution

Michael Nayhouse [a], Anh Tran [a], Joseph Sang-Il Kwon [a], Marquis Crose [a],
Gerassimos Orkoulas [b], Panagiotis D. Christofides [a,c,*]

[a] Department of Chemical and Biomolecular Engineering, University of California, Los Angeles, CA 90095, USA
[b] Department of Chemical Engineering, Widener University, Chester, PA 19013, USA
[c] Department of Electrical Engineering, University of California, Los Angeles, CA 90095, USA

HIGHLIGHTS

- Multiscale modeling of ibuprofen batch crystallization.
- Calculation of evolution of ibuprofen crystal shape distribution.
- Model predictive control of ibuprofen crystal shape distribution.
- Comparison with standard control policies.

ABSTRACT

In this work, we focus on multiscale modeling and control of a seeded batch crystallization process used to produce ibuprofen crystals. For the modeling of the crystal growth process, we consider kinetic Monte Carlo (kMC) simulations comprising of molecule adsorption, desorption, and migration type microscopic surface events. To account for growth rate variability, we propose a model for growth rate dispersion (GRD), based on the available experimental data, which will be applied at the individual crystal growth level in the kMC simulations. Finally, a model predictive controller (MPC) is developed in order to control the crystal size distribution of ibuprofen in the batch crystallization process and the MPC closed-loop performance is compared against constant temperature control (CTC) and constant supersaturation control (CSC) policies. The proposed MPC is able to deal with the constraints of the control problem, in addition to minimizing the spread of the crystal size distribution in a superior fashion compared to the other control methodologies, which improves the crystal product quality at the end of the batch.

© 2015 Elsevier Ltd. All rights reserved.

1. Introduction

Crystallization is a key separation process in the pharmaceutical industry which is estimated to be over a $1 trillion per year industry. It is used for drug purification, separation, and preformulation. A key consideration in crystallization is that in order to achieve desired crystal product quality, the process environment must be controlled appropriately. Otherwise, the target drug could lose purity, stability, and bio-availability.

Simulation techniques are valuable tools that can be used in crystal growth modeling which usually consist of equilibrium Monte Carlo (MC) and kinetic Monte Carlo (kMC) simulations, as well as molecular dynamics (MD) simulations (Lovette et al., 2008). A well-written book by Frenkel and Smit (2002), in addition

to a review by Rohl (2003), goes into detail about the development of these simulation techniques. In regards to crystallization, MD simulations are quite helpful when looking at how molecules move and how they are incorporated into the crystal, however, the length and time scales of MD simulations make them difficult to use for process modeling (Lovette et al., 2008). On the other hand, kMC simulations allow for more realistic length and time scales by using rate equations that describe different microscopic phenomena. To this end, kMC simulation methods have been widely used to simulate molecular-level phenomena like crystal nucleation, growth, and aggregation (Bortz et al., 1975; Dai et al., 2005, 2008; Gillespie, 1976, 2007; Rathinam et al., 2003; Reese et al., 2001; Snyder et al., 2005; Gilmer and Bennema, 1972; Kwon et al. 2013a, b, 2014; Jolliffe and Gerogiorgis, 2015). Furthermore, kMC simulation methods have been successfully applied to compute the net crystal steady-state growth rate accounting for the dependence of the desorption and migration rates on the local surface microconfiguration. For that reason, we look to investigate the batch crystal growth process of ibuprofen, one of the most widely used

non-steroidal anti-inflammatory drugs (NSAID), via kMC simulations in this work. Due to the lack of availability of primary nucleation rate data, we will consider a seeded batch crystallization process and keep the supersaturation at low enough levels that the impact of nucleation and crystal fines formation will be minimal compared to the amount of crystals seeded to the system.

Ibuprofen works by reducing prostaglandins, which are the hormones causing inflammation and pain in the body. These are usually referred to as local hormones since they only act close to the location where they are produced. Although they are helpful initially since swelling will restrict injured areas and increased blood flow will assist in healing, longer term pain is undesirable. Thus, many different types of painkillers are used, where ibuprofen is one of the most common and widely available choices. In the US, ibuprofen brand Advil was the top over the counter (OTC) brand by revenue in 2013 with just over $490 million.

More specifically, we first model the ibuprofen crystal growth process. In order to do this, we investigate the growth rates of the (001) and (011) faces via a kMC simulation model. To account for variability in experimental crystal growth rate data, we develop a model for growth rate dispersion (GRD) since this phenomenon is known to affect ibuprofen crystal growth rates and this model is applied at the individual crystal level. After that, a seeded batch crystallizer will be considered, requiring the development of mass and energy balances for the modeling of the continuous-phase variables and this macroscopic model is combined with the microscopic crystal growth model. Finally, the crystal size distribution will be controlled by a model predictive controller (MPC) and compared against classical control strategies used in industry.

2. Ibuprofen crystal growth

2.1. Kinetic Monte Carlo modeling and simulation

In the present work, we will use kinetic Monte Carlo (kMC) simulations in order to model the growth rates of ibuprofen crystal faces since crystal growth is a non-equilibrium process. Unlike equilibrium Monte Carlo simulations, kMC simulations add an element of time by using rate equations representing different microscopic phenomena. Furthermore, this allows modeling the dependency of the crystal growth rates on the surface micro-configuration, in addition to the ability to consider individual crystals, thereby allowing for a more realistic model for growth rate dispersion. Ibuprofen has unit cell parameters of $a = 14.397$ Å, $b = 7.818$ Å, $c = 10.506$ Å, and $\beta = 99.70°$ with four molecules per unit cell (Shankland, 1996; Shankland and Wilson, 1997). For this work, we will consider an $N \times N$ lattice with one molecule per lattice site and periodic boundary conditions. The types of microscopic events we consider in our kMC simulations in order to model the crystal growth are adsorption, desorption and migration. Nearest neighbor lists will be used to aid the computational efficiency when calculating the total rates for each of the microscopic phenomena (Christofides et al., 2008). The rate equations considered in this work are set up similar to that of Durbin and Feher (1991) for lysozyme, however, they have been modified to account for available growth rate data of ibuprofen on the (001) and (011) faces (Nguyen et al., 2014). Cano et al. (2001) reported data for all three faces (i.e., (001), (011), and (100)), however, they conducted their experiments at very low supersaturation ($\sigma = 0.013$) which is much lower than the supersaturation range of our study ($0.68 \leq \sigma \leq 1.20$), and thus, we were not able to use their data for comparison purposes in the present study. If more data becomes available in the future for the (100) face, then the dynamics of the (100) face can easily be integrated into the present kMC simulation model.

2.2. Rate equations

The per-site adsorption rate is defined as

$$r_a = K_a \sigma, \tag{1}$$

where K_a is the adsorption coefficient and σ is the relative supersaturation of the system defined by the following equation:

$$\sigma = \frac{\dfrac{I}{E} - \dfrac{I^*}{E}}{\dfrac{I^*}{E}}, \tag{2}$$

where I is the ibuprofen content, E is the ethanol content, and I^*/E is the solubility. The solubility will be taken from Rashid et al. (2008, 2011) and is defined as

$$\frac{I^*}{E} = 0.497 + 0.001026T^2, \tag{3}$$

with temperature T defined in degrees Celsius. Since we consider an $N \times N$ lattice model, the total rate of adsorption is simply

$$W_a = N^2 r_a. \tag{4}$$

Unlike adsorption, the rates of desorption and migration will be dependent on the local environment at each lattice site (i.e., number of nearest neighbors to this site). When a particle has a high number of nearest neighbors, a lower desorption/migration rate will be associated with this site due to the fact that the particle is more stable in its current location. Likewise, when a particle has very few or no nearest neighbors, that particle will have a higher desorption/migration rate. Thus, we will use an Arrhenius type equation for the per-site rate of desorption, r_d, which is defined as follows:

$$r_d(i) = K_d \exp\left(-i\frac{E_{pb}}{k_B T}\right), \tag{5}$$

where K_d is the desorption coefficient, i is the number of nearest neighbors for the current lattice site ranging from zero to four (N, S, E, W directions), E_{pb} is the binding energy per bond, k_B is the Boltzmann constant, and T is the temperature in Kelvin. In order to find the total rate of desorption, we sum over the entire lattice. This can be done in a simple way by taking advantage of the fact that there are five different types of local environments, rather than checking each individual lattice site requiring an $O(N^2)$ calculation. Thus, the total rate of desorption is

$$W_d = \sum_{i=0}^{4} W_{d_i}, \quad W_{d_i} = M_i r_d(i), \tag{6}$$

where W_{d_i} is the total rate of desorption for lattice sites with i nearest neighbors and M_i is the number of lattice sites with i nearest neighbors. Migration works in an analogous way and is defined as follows:

$$r_m(i) = K_m \exp\left(-i\frac{E_{pb}}{k_B T}\right), \tag{7}$$

$$W_m = \sum_{i=0}^{4} W_{m_i}, \quad W_{m_i} = M_i r_m(i), \tag{8}$$

where r_m is the per-site rate of migration, K_m is the migration coefficient, W_m is the total rate of migration, and W_{m_i} is the total rate of migration for lattice sites with i nearest neighbors. Lastly, the amount of time elapsed when an event occurs is defined in the following way:

$$\Delta t = -\ln(1 - \zeta)/W_{\text{tot}}, \tag{9}$$

where ζ is a uniform random number, i.e., $\zeta = [0, 1)$, and $W_{\text{tot}} = W_a + W_d + W_m$.

A coarse-grained model could be adequate for the purpose of computing the crystal growth rate. However, the kMC simulation is employed to compute the net crystal growth rate accounting for the dependence of surface migration and detachment rates on the surface micro-configuration. Furthermore, the evolution of the crystal shape, which is represented by the ratio between the heights in the direction of the (011) and (001) faces, is modeled through the kMC simulation. Lastly, the kMC simulation can be used to predict the crystal growth dynamics at the operating conditions where experimental data are not available.

2.3. Growth rate dispersion

Growth rate dispersion (GRD) is a well-known phenomenon where crystals of the same type, undergoing seemingly the same conditions, grow at different rates. More specifically, growth rate dispersion is defined as the variation in growth rates under fixed thermodynamic and hydrodynamic conditions. The growth of crystals is mainly caused by the transfer of solute molecules from the bulk to the kink sites on the crystal surfaces. Therefore, the growth rates of the different crystals are determined by the interplay between the mechanism of kink site formation and the transport of solute molecules to the crystal surface, both of which are stochastic processes. Furthermore, the densities of kink sites and their evolution are functions of the temperature and supersaturation but also functions of the surface micro-configurations (Garside, 1985; Zacher and Mersmann, 1995; Judge et al., 2010; Randolph and White, 1977; Garside and Ristic, 1983; ÓMeadhra and van Rosmalen, 1996). Previous models that describe this process include the constant crystal growth (CCG) model (Garside, 1985; Larson et al., 1985), the random fluctuation (RF) model (Randolph and White, 1977), and the fast growers, slow growers (FGSG) model (Daudey, 1987; Rusli et al., 1980; Garside and Ristic, 1978). In the CCG model, a distribution of crystals has a distribution of growth rates and individual crystals adhere to a specific growth rate from that distribution during the entire period of growth (Larson et al., 1985). The RF model requires individual crystal growth rates to fluctuate around an average value. Lastly, the FGSG model states that small crystals will grow at lower growth rates compared to the larger ones. In the present work, we account for GRD in a way that is similar to the constant crystal growth (CCG) model by randomly giving each crystal a uniform random number, ζ_{GRD}, at the start of the simulation of each crystal growth process, which will be used to calculate the GRD factor for each crystal. More specifically, GRD_f for each crystal will be computed separately in the following way:

$$GRD_f = 2\frac{C_{GRD}}{\sigma}\zeta_{GRD} + \left(1 - \frac{C_{GRD}}{\sigma}\right), \tag{10}$$

where C_{GRD} is the GRD constant and will be calculated to fit experimental data of ibuprofen crystal growth rate dispersion. It is noted that GRD_f is dependent on σ due to the fact that error bars became too small at lower supersaturation values and too large at higher supersaturation values when fitting to experimental data without having this dependence. The results of this fit are presented in the next subsection. The GRD factor will affect the rate of adsorption (i.e., each crystal will have a slightly different rate of adsorption depending on the ζ_{GRD} assigned to that crystal at the start of the simulation). This will allow for variation in the growth rates in a manner consistent with the experimentally computed values and it will be explicitly defined in the following way in this work:

$$\sigma_{GRD} = \sigma GRD_f. \tag{11}$$

It is noted that in order for this change to take place, σ_{GRD} will replace σ in Eq. (1) to give

$$r_a = K_a\sigma_{GRD}. \tag{12}$$

We used the kinetic Monte Carlo model to describe the crystal growth rate process determined by surface mechanisms such as solute molecule adsorption, migration, and desorption processes. Then, this microscopic model is integrated with the macroscopic model such as mass and energy balance equations for the crystallizer to construct the multiscale process model which is used to simulate the batch crystallization process. Within this context, the minor fluctuation in the protein solute concentration and the temperature in the crystallizer due to Brownian motion are disregarded. In the future, by adopting a molecular level approach, we could directly model the growth rate dispersion in the crystallizer at a molecular level. Comprehensive reviews on multiscale modeling can be found in Weinan et al. (2003), Vlachos (2005), Christofides et al. (2008), Ricardez-Sandoval (2011).

2.4. Fitting the kMC model parameters to experimental results

For a given set of simulation conditions comprised of temperature, ibuprofen content, ethanol content, and water content, the kMC simulation methodology and GRD model described earlier in this section result in growth rate values of ibuprofen for the (001) and (011) faces over a range of supersaturations. In Fig. 1, ibuprofen crystal growth rates are modeled at 95% ethanol, $I/E = 2$, and a relative supersaturation range of $0.68 \lesssim \sigma \lesssim 1.20$. The growth rates at each point in the kMC are produced by averaging 640 independent crystal runs with the error bars representing the standard deviation. Results are compared to experimental growth rates at 95% ethanol from Nguyen et al. (2014), as well as a best fit line given by Rashid et al. (2012) which has the equation $G = k_G s$, where $k_G = 15$ and $s = (I/E) - (I^*/E)$. While Rashid et al. (2012) give an overall growth rate for the crystals, Nguyen et al. (2014) present the growth rate data in the direction of the (001) and (011) faces separately.

The model parameters used for the kMC simulations are listed in Table 1. Additionally, C_{GRD} was found to be 0.07 resulting in an average coefficient of variation (CV) for the kMC simulation data to be 0.14, compared to 0.12 given in Nguyen et al. (2014). Also, the kMC growth rate data for the (001) and (011) faces were fit using a least squares linear regression model which will be used later in the model predictive controller. The results of this fit are
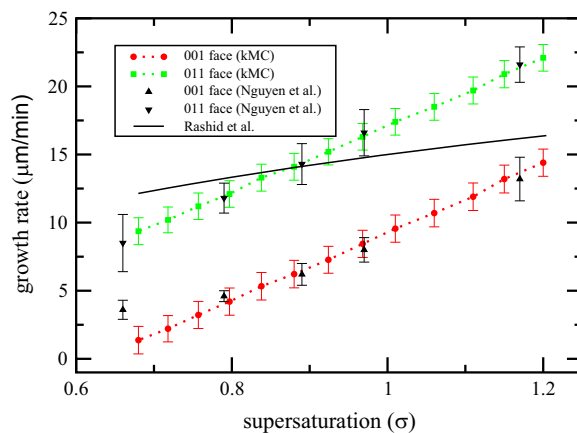
$$G_{001} = 24.843\sigma - 15.564, \tag{13}$$

Fig. 1. Growth rate versus supersaturation for the (001) and (011) faces for the kMC model. Additionally, the experimental results from Nguyen et al. (2014) and the trendline from Rashid et al. (2012) are shown.

and

$$G_{011} = 24.412\sigma - 7.2772. \tag{14}$$

It is noted that size effects of the lattice were considered and results from $N=15$ and larger were consistent and showed no change in results. So, for this work N was set to 20 in order to ensure consistency without being too large, thereby causing an exponential increase in required simulation time. In this work, the effect of lattice size used in the kMC simulation on the crystal growth rate is minimal in comparison to the effect of lattice sized used in the kMC on the surface roughness of the crystal surface (a variable that is not of interest in the present work; the interested readers may find more information in Hu et al., 2009). Therefore, we can disregard the finite size effect of the lattice size on the growth rate.

3. Batch crystallization

3.1. Energy and mass balance equations

The energy and mass balance equations which calculate the change in temperature, T, and ibuprofen content, I, are given by the following ordinary differential equations:

$$\frac{dT}{dt} = -\frac{\rho_c \Delta H_c}{\rho_{\text{slurry}} C_p V_{\text{slurry}}} \frac{dV_c}{dt} - \frac{U_j A_j}{\rho_{\text{slurry}} C_p V_{\text{slurry}}} (T - T_j), \quad T(0) = T_0, \tag{15}$$

$$\frac{dI}{dt} = -\rho_c \frac{dV_c}{dt}, \quad I(0) = I_0, \tag{16}$$

where ρ_c is the density of the crystal phase, ΔH_c is the enthalpy of crystallization, ρ_{slurry} is the density of the slurry phase, C_p is the specific heat capacity, V_{slurry} is the volume of the slurry phase, V_c is the total volume of all the crystals, t is the time, U_j and A_j are the overall heat transfer coefficient and area between the jacket stream and the crystallizer, respectively, and T_j is the temperature of the jacket stream. Additionally, T_0 and I_0 are the starting temperature and ibuprofen content of the batch system, respectively. The values for these parameters are given in Table 2.

Adding an energy balance equation in order to take into account the jacket temperature dynamics would not significantly modify the practical implementation of the controller.

Table 1
Parameters for faces (001) and (011) at $I/E = 2$.

Parameter	Value	Units
E_{pb}/k_B (001)	17.47	K
E_{pb}/k_B (011)	125.20	K
K_a	380	s^{-1}
K_d	270	s^{-1}
K_m	300	s^{-1}

Table 2
Parameters for faces (001) and (011) at $I/E = 2$. Note that the ranges are given for the slurry density and specific heat capacity since they are calculated by composition of the slurry throughout the entire simulation. The model parameters are adopted from Shi et al. (2006) and Nguyen et al. (2014).

Parameter	Description	Value	Units
ρ_c	Crystal density	1030	mg/cm^3
ΔH_c	Enthalpy of crystallization	-112.95	kJ/kg
ρ_{slurry}	Slurry density	485–510	mg/cm^3
C_p	Specific heat capacity	1.85–2.0	J/g K
A_j	Surface area of crystallizer wall	0.25	m^2
U_j	Heat transfer coefficient of crystallizer wall	1800	kJ/m^2 h K

3.1.1. Volume calculation

In order to properly calculate the mass and energy balance terms that require volume change information, we first need to accurately estimate the volume of the ibuprofen crystals. In order to do this, we need to know the height for all three faces (i.e., (001), (011), and (100)), along with the interfacial angle α. Since we explicitly model the growth rates for the (001) and (011) faces, we can easily determine the heights of the (001) and (011) faces. On the other hand, for the (100) face, we will use visual approximation from Rasenack and Müller (2002) to estimate its relative height. The results of this approximation show that the (100) face is roughly 4–8 times slower growing than the (001) face. Thus, we will assume:

$$h_{100} \cong \frac{h_{001}}{6}, \tag{17}$$

where h_{100} and h_{001} are the heights of the (100) and (001) faces, respectively. Second, we will use the images provided in Nguyen et al. (2014) in order to measure the interfacial angle, α, as a function of supersaturation. Using these images, we found the following relationship:

$$\alpha = -14.368°\sigma + 105.41°. \tag{18}$$

With the use of Eqs. (17) and (18), the volume of each crystal (see e.g., Fig. 2) can now be calculated in the following way:

$$V_{\text{crystal}} = \frac{4h_{001}}{\sin\left(\frac{\alpha}{2}\right)} \left(2h_{011} - h_{001} \cos\left(\frac{\alpha}{2}\right)\right) h_{100}. \tag{19}$$

We used the kMC model to describe the crystal growth rate process at the microscopic level accounting for surface mechanisms such as solute molecule adsorption, migration, and desorption processes, as well as accounting for growth rate dispersion. Then, this microscopic model was integrated with the macroscopic model such as mass and energy balance equations to construct the multiscale process model which is used to simulate the batch crystallization process.

4. Model predictive control

In the seeded batch crystallization process of ibuprofen, kMC simulations are considered for the crystal growth process via adsorption, desorption, and migration type microscopic surface events. The growth rates produced by these simulations are
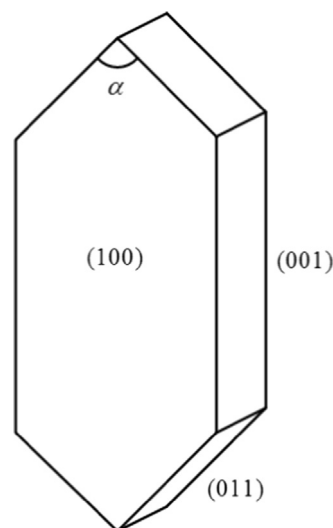

Fig. 2. Geometry of the ibuprofen crystal. Labels show the (100), (001), and (011) faces, as well as the interfacial angle, α.

directly related to the supersaturation of the system, which can be modified by changing the temperature of the jacket which is in contact with the batch reactor. In this section, a model predictive controller (MPC) is presented for seeded batch ibuprofen crystallization control. MPC is used in order to provide optimality, robustness, and constraint handling in the batch crystallization process (Shi et al., 2006, 2005; Kwon et al., 2014). In particular, the objective of the MPC will focus on minimizing the crystal size distribution by computing a set of optimal jacket temperatures over the length of the prediction horizon. The main reason for shape control is not directly considered in this work due to the fact that the shape of ibuprofen crystals is more dependent on the solvent choice rather than the batch temperature. Additionally, an actuator constraint on the rate of change of the jacket temperature is imposed, as well as a constraint on the temperature and supersaturation of the system so that crystallization will take place in an appropriate environment to avoid damaging the crystal. Furthermore, the growth rates will be modeled via Eqs. (13) and (14) in the MPC. Lastly, the energy and mass balance equations are considered (i.e., Eqs. (15) and (16)). The formulation for the MPC developed in this work is as follows:

$$\underset{T_{j,1},\ldots,T_{j,i},\ldots,T_{j,p}}{\text{minimize}} \quad \sum_{i=1}^{p} \left(\left(V_{\text{set}} - \frac{M_1}{M_0} \right) \Big/ V_{\text{set}} \right)^2$$

$$\text{subject to} \quad \frac{dM_1}{dt} = G_{\text{vol}} M_0, \quad M_0 = 5 \times 10^6$$

$$G_{001} = 24.843\sigma - 15.564, \quad G_{011} = 24.412\sigma - 7.2772$$

$$G_{100} = \frac{G_{001}}{6}$$

$$\sigma = \frac{\frac{I}{E} - \frac{I^*}{E}}{\frac{I^*}{E}}, \quad \frac{I^*}{E} = 0.497 + 0.001026T^2$$

$$\langle V_{\text{crystal}} \rangle = \frac{4\langle h_{001} \rangle}{\sin\left(\frac{\alpha}{2}\right)} \left(2\langle h_{011} \rangle - \langle h_{001} \rangle \cos\left(\frac{\alpha}{2}\right) \right) \langle h_{100} \rangle$$

$$\langle h_k \rangle = \langle h_k(t_{i-1}) \rangle + G_k \Delta$$

$$\frac{dT}{dt} = -\frac{\rho_c \Delta H_c}{\rho_{\text{slurry}} C_p V_{\text{slurry}}} \frac{dM_1}{dt} - \frac{U_j A_j}{\rho_{\text{slurry}} C_p V_{\text{slurry}}} (T - T_j), \quad T(0) = T_0$$

$$\frac{dI}{dt} = -\rho_c \frac{dM_1}{dt}, \quad I(0) = I_0$$

$$T_{\min} \le T \le T_{\max}, \quad \left| \frac{T_{j,i+1} - T_{j,i}}{\Delta} \right| \le 2.0 \,°\text{C/min}$$

$$\sigma_{\min} \le \sigma \le \sigma_{\max}$$

$$i = 1, 2, \ldots, p, \quad k \in \{001, 011, 100\} \tag{20}$$

where $p = 10$ is the length of the prediction horizon, $\Delta = 40$ is the sampling time in seconds, V_{set} is the desired average volume set point, $\langle V_{\text{crystal}} \rangle$ is the average volume of the crystal distribution, T_j is the jacket temperature, $T_{j,i}$ is the jacket temperature at the ith prediction step, $\langle h_k \rangle$ is the average height on face k, and M_0 and M_1 are the zeroth and first moments of the crystal size distribution, respectively. M_0 represents the total number of crystals and M_1 represents the total volume of the crystals. It is noted that since we consider a seeded batch crystallizer without nucleation, M_0 will be constant for this work. If nucleation data were available, then it follows that M_0 would need to be a variable in the control problem given by Eq. (20) and more considerations would be taken to attempt to minimize the presence of crystal fines. Additionally, G_{vol} is the volumetric growth rate and is calculated by finding the change in average crystal volume. Finally, values of $\sigma_{\min} = 0.6$, $\sigma_{\max} = 1.3$, $T_{\min} = 10\,°\text{C}$, and $T_{\max} = 40\,°\text{C}$ are used for this work. The set of optimal jacket temperatures along the prediction horizon is obtained by solving Eq. (20) in a receding horizon fashion with IPOPT, an open source software package for large-scale nonlinear optimization. The first value, $T_{j,1}$, is then applied to

the system until the next sampling time when a new set of optimal jacket temperatures is calculated.

The interested readers may find more detailed analysis and handling of the effect of model parameter uncertainty on the optimal jacket temperature trajectories in Rasoulian and Ricardez-Sandoval (2014, 2015) and Kwon et al. (2015).

5. Closed loop simulations

For the seeded batch crystallization simulations, we investigate the crystal size and shape distributions. The same initial conditions, other than starting temperature, are used in every simulation to ensure consistency. For this work, the initial conditions of the seeded batch reactor are $V_{\text{solvent}} = 400$ mL (95% ethanol), $I/E = 2$, $I_{\text{start}} = 6 \times 10^5$ mg, and $M_0 = 5 \times 10^6$. Each of the simulations is completed when the average crystal volume reaches the set point, $V_{\text{set}} = (150\,\mu\text{m})^3 = 3.375 \times 10^6\,\mu\text{m}^3$.

Due to the nature of the batch process and the dependence of the growth rate on the supersaturation and temperature trajectories, the time to finish each simulation will vary. To deal with this, we will consider a normalized time to compare the different simulations, i.e., 0 at the start of the simulation and 1 when the batch has reached V_{set}. Also, it is noted that the kMC simulations are run with constant batch parameters (i.e., temperature, ibuprofen content, and supersaturation) for 0.333 s. At that point, Eqs. (15) and (16) are calculated, all system parameters are updated, and this process is repeated until the end of the simulation.

5.1. MPC performance

In this subsection, we investigate the closed-loop performance of the proposed MPC scheme to regulate the volume and shape distributions of ibuprofen crystals produced from a seeded batch crystallization process. Specifically, we look at the effect of different initial temperatures and growth rate dispersion on the size and shape distributions of ibuprofen crystals. We consider starting temperatures ranging from 15 °C to 30 °C with a step size of 5 °C. The crystal volume distribution for each of the cases is shown in Fig. 3. What can be noticed is that the lower starting temperatures lead to a slightly more narrow size distribution. This is due to the fact that lower temperatures correspond to higher supersaturation values, and at these higher supersaturation values the relative effect of the GRD is less compared to the effect of GRD on lower supersaturation values (see e.g., Fig. 1). The differences in each of the starting conditions become much more noticeable in Fig. 4 which shows the crystal shape distribution. We define the
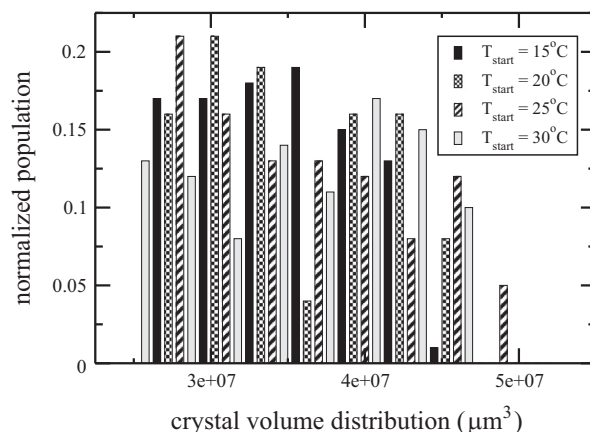

Fig. 3. Crystal volume distribution for MPC showing results for starting temperatures 15 °C, 20 °C, 25 °C, and 30 °C.
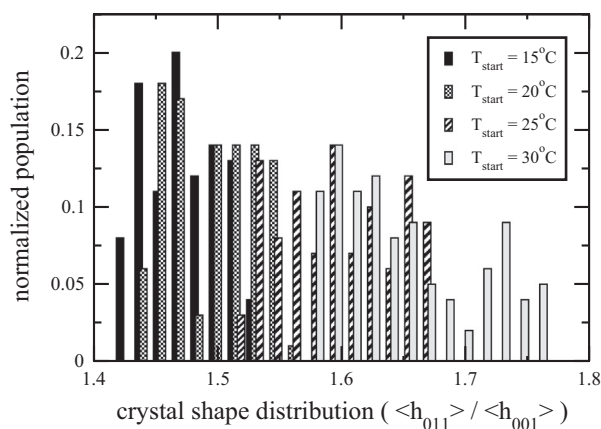
Fig. 4. Crystal shape distribution for MPC showing results for starting temperatures 15 °C, 20 °C, 25 °C, and 30 °C.

crystal shape to be the relative average height of the (011) face to the (001) face since the (100) face is determined by Eq. (17). The crystal shape distribution not only becomes wider as the starting temperature gets higher, but also it shifts to the right meaning that the crystals become more elongated. Again, when looking at Fig. 1, it is evident that the ratio between the (011) and (001) faces is greater at lower values of supersaturation (i.e., higher values of temperature) which results in an elongated crystal shape for the higher starting temperatures in Fig. 4. Looking at Fig. 5, we can infer a more detailed view of the dynamics of the batch crystallizer conditions. What is important to notice is that MPC is able to successfully deal with the constraints of the system (e.g., $T_{start} = 15$ °C or 30 °C where the supersaturation starts outside of the supersaturation constraint region). Furthermore, after the MPC has changed the batch temperature from the initial starting temperature, each of the different simulations follows a path that resembles crystallizer cooling. This is done since as the crystallization progresses, ibuprofen content will go from the slurry phase to the crystal phase causing a decrease in concentration (i.e., I/E). In order to balance this effect and keep the supersaturation from falling to very low values, the temperature is lowered in order to keep the crystal growth progressing.

5.2. Comparison of MPC performance with other control strategies

In order to compare the performance of the proposed MPC, we performed additional simulations using constant temperature control (CTC) and constant supersaturation control (CSC) strategies. For these simulations, we chose the starting temperature $T_{start} = 20$ °C for CTC, CSC, and MPC which corresponds to a starting supersaturation $\sigma \cong 1.2$. This starting point was chosen to ensure both CTC and CSC would be in a valid operating region accounting for the desired supersaturation and temperature ranges since these control methods are unable to deal with constraints. The crystal volume distribution can be seen in Fig. 6. It is clear that CTC leads to the most broad crystal size distribution and it can be seen that MPC gives a slightly more narrow distribution than CSC. Similar behavior is seen in Fig. 7 for the shape distribution where CSC and CTC shift the crystal shape distribution to the right compared to the MPC. MPC produces the most narrow crystal size distribution due to the jacket temperature trajectory it chooses and due to its ability to work within a constrained region. Additionally, the way the MPC goes about minimizing the volume distribution also happens to produce the most narrow crystal shape distribution.

The differences in each of these policies are highlighted when looking at the dynamics of the batch reactor in Fig. 8. As expected,
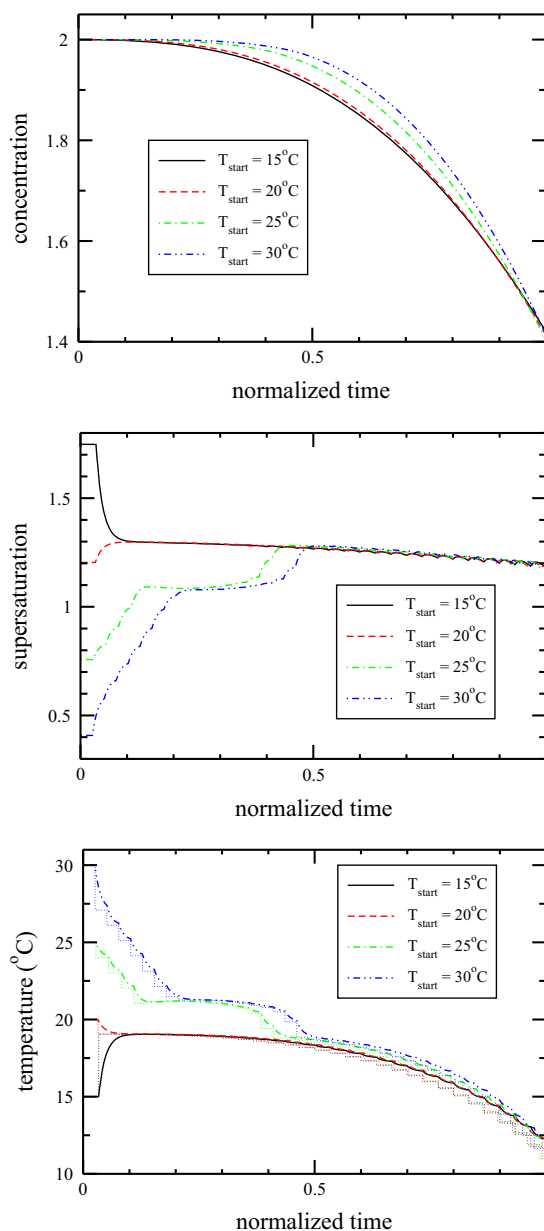

Fig. 5. Concentration, supersaturation, and temperature versus normalized time for MPC showing results for starting temperatures 15 °C, 20 °C, 25 °C, and 30 °C. For the temperature plot, the dotted lines represent the jacket temperature, T_j, for each of the runs.
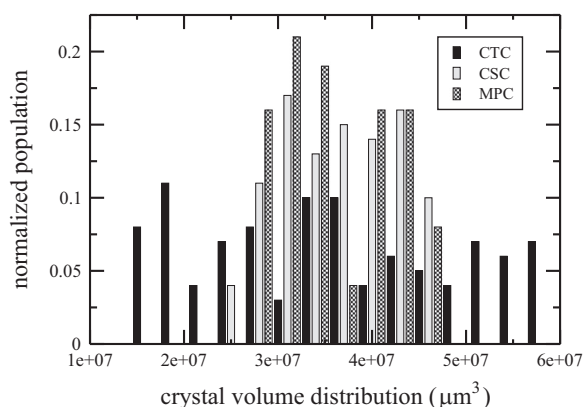

Fig. 6. Crystal volume distribution for CTC, CSC, and MPC at the end of the batch.
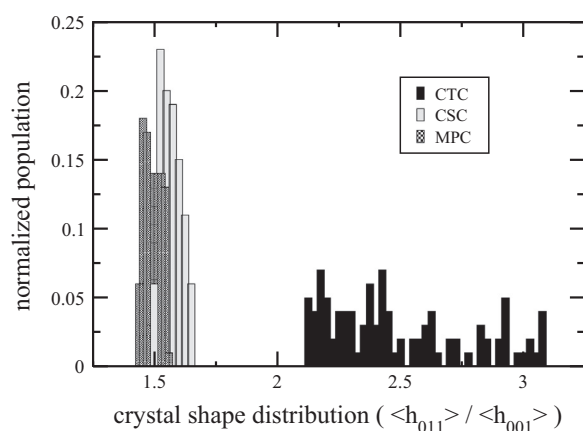
Fig. 7. Crystal shape distribution for CTC, CSC, and MPC at the end of the batch. Note that one bar from CSC has been placed in front of MPC due to the fact that it was completely covered by the MPC bars.

CTC holds the jacket temperature at 20 °C throughout the entire simulation, however, it is noted that the supersaturation drops significantly below 1.2 in the CSC policy. This is due to the actuator constraint on T_j thereby limiting the maximum rate of change and causing the supersaturation to drop. It is also interesting to note that MPC and CSC take nearly identical pathways in terms of concentration to reach the desired set-point. Overall, MPC is able to outperform other techniques since it is able to "plan ahead" and predict what will happen next which is especially important when there is significant concentration drop in the system.

GRD of individual crystal faces, which is modeled as a function of supersaturation by using the coefficient of variation of the corresponding facet growth rate, decreases with an increase in supersaturation. Therefore, when the controller primary objective is to lessen the influence of GRD on the final CSD (by explicitly penalizing the GRD in the cost function), the ibuprofen batch crystallization process is operated constantly by the controller in high supersaturation regime. The operating strategy of such an MPC however is identical to that of the MPC used in the present work whose primary objective is to achieve the shortest operating time that leads to the desired average crystal size. Furthermore, in this work, due to the lack of ibuprofen primary nucleation rate data, the maximum allowable supersaturation level inside the batch crystallizer is determined to be 1.3 in order to minimize the primary nucleation and its impact on the CSD. It is also worth mentioning that due to the exponential decay dependence of the GRD of the (001) face on the supersaturation, the GRD of the (001) face can change significantly with a small fluctuation in supersaturation. Due to this fact and the operating constraint of how quickly temperature of the crystallizer can be adjusted, and the fact that larger crystals deplete the solute concentration in continuous phase faster than smaller crystals, the MPC penalizing GRD explicitly in its cost function becomes more sensitive to the size of the sampling time interval because a slight change in the supersaturation level during sampling time can have a significant impact on the value of the cost function. Simulation data (not reported here for brevity) confirm that changing the cost function to add penalty on GRD would only make the controller more sensitive to sampling time and more complicated without leading to a different operational behavior that would reduce CSD polydispersity further.

5.3. Computational performance and scaling

To close out this section, it is important to note the computational performance and scaling for this work. In order to make this
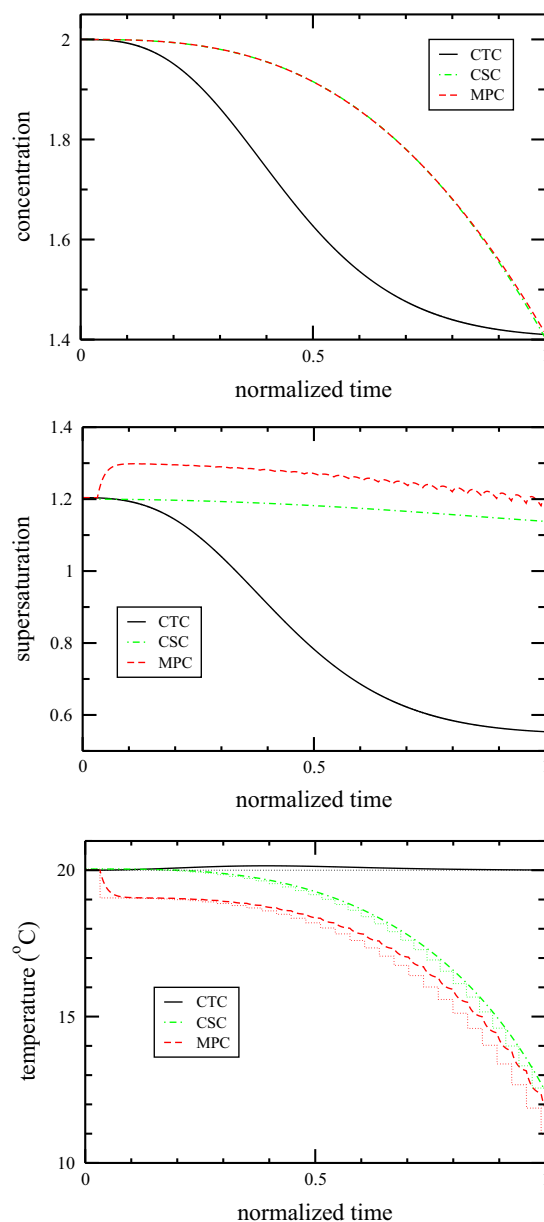

Fig. 8. Concentration, supersaturation, and temperature versus normalized time for CTC, CSC, and MPC. For the temperature plot, the dotted lines represent the jacket temperature, T_j, for each of the runs. Additionally, it is noted that both CSC and MPC follow a very similar path in the concentration plot until the very end.

comparison, we ran the same seeded batch crystallization simulation and initial conditions with different random seeds on the Texas Advanced Computing Center's Stampede cluster. The code was optimized using Message Passing Interface (MPI) over the crystal growth stage since it was determined to be the bottleneck of this simulation. Specifically, at the start of the simulation, crystals are assigned to one of the available cores. Next, the growth process runs while the batch system parameters remain constant until it is time to update the crystallizer conditions. After these parameters are updated, the crystals will go back into the growth stage on their assigned core. This process is repeated until the end of the simulation. The results of these simulations for varying number of cores are shown in Fig. 9 and the data points are given in Table 3. What can be seen from Fig. 9 is that there is a significant decrease in time required to complete the batch simulation as the number of cores are increased. Looking at Table 3, it is evident that as the number of cores is doubled, the
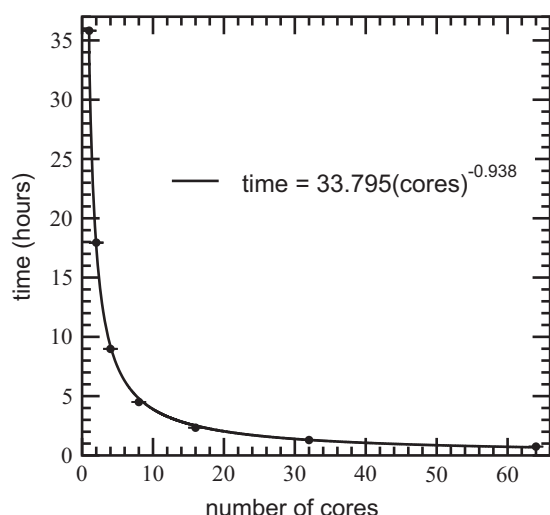
Fig. 9. The number of cores versus the average amount of time required to finish the batch simulation. Error bars are shown as one standard deviation over 10 simulations for each batch run. The best fit line has equation: time $= 33.795$cores$^{-0.938}$ with an $R^2 = 0.9982$.

Table 3

The time to finish each simulation for varying number of cores and the corresponding speedup and strong scaling. Note that the speedup is defined as $(t_1 - t_n)/t_1$, where t_1 is the time the process takes on 1 core and t_n is the time the process takes on n cores.

Cores	Time (h)	Speedup (%)	Strong scaling (%)
1	35.82	0.0	100.0
2	17.95	49.9	99.8
4	8.98	74.9	99.7
8	4.50	87.4	99.4
16	2.34	93.5	95.6
32	1.30	96.4	86.2
64	0.75	97.9	74.8

simulation time goes down by about half. In order to further analyze the scalability of this parallel process, it is useful to analyze the strong scaling behavior, which is defined as

$$S_{\text{strong}} = \frac{t_1}{n_{\text{cores}} t_n}, \tag{21}$$

where t_1 is the time the process takes on 1 core, n_{cores} is the number of cores, and t_n is the time the process takes on n cores. Strong scaling is good for analyzing systems like this one that are CPU bound, showing how well the process can be parallelized without adding too much wasted time in overhead costs. From Table 3, it can be seen that the strong scaling stays above 90% when using 16 or fewer cores and drops down afterwards. This is likely due to the fact that simulations were run on compute nodes which had 16 cores per node (two 8-core CPUs) and when going over 16 cores, communication must then take place between multiple nodes, thus adding overhead costs. Overall, it is clear from both Fig. 9 and Table 3 that the batch crystallization process of ibuprofen is greatly benefiting from the use of MPI for the kMC process.

6. Conclusions

In this work, we studied the seeded batch crystallization process of ibuprofen. First we used kMC simulations to develop a growth rate model which also accounts for GRD. Next, we proposed an MPC strategy in order to control the crystal size distribution. Lastly, we compared the proposed MPC strategy to CTC and CSC policies. We found that the MPC is able to deal with constraints and a wide variety of starting conditions for ibuprofen crystal growth. Additionally it was found that MPC produced more narrow volume and shape distributions compared to the other control strategies which is important because the product quality is directly determined by the final crystal size and shape distributions. It is important to note that the growth rate dispersion is mainly responsible for the wide distribution ranges seen in this work. Lastly, we found an extreme benefit in the use of MPI for this work due to heightened CPU time requirements.

References

Bortz, A.B., Kalos, M.H., Lebowitz, J.L., 1975. New algorithm for Monte Carlo simulation of Ising spin systems. J. Comput. Phys. 17, 10–18.

Cano, H., Gabas, N., Canselier, J.P., 2001. Experimental study on the ibuprofen crystal growth morphology in solution. J. Cryst. Growth 224, 335–341.

Christofides, P.D., Armaou, A., Lou, Y., Varshney, A., 2008. Control and Optimization of Multiscale Process Systems. Birkhäuser, Boston.

Dai, J., Kanter, J.M., Kapur, S.S., Seider, W.D., Sinno, T., 2005. On-lattice kinetic monte carlo simulations of point defect aggregation in entropically influenced crystalline systems. Phys. Rev. B 72, 134102.

Dai, J., Seider, W.D., Sinno, T., 2008. Coarse-grained lattice kinetic Monte Carlo simulation of systems of strongly interacting particles. J. Chem. Phys. 128, 194705.

Daudey, P.J., 1987. Crystallization of Ammonium Sulfate (PhD dissertation). Delft University of Technology, The Netherlands.

Durbin, S.D., Feher, G., 1991. Simulation of lysozyme crystal growth by the Monte Carlo method. J. Cryst. Growth 110, 41–51.

Frenkel, D., Smit, B., 2002. Understanding Molecular Simulation. Academic Press, New York.

Garside, J., 1985. Industrial crystallization from solution. Chem. Eng. Sci. 40, 3–26.

Garside, J., Ristic, R.I., 1978. Direct observation of secondary nuclei production. J. Cryst. Growth 43, 694–704.

Garside, J., Ristic, R.I., 1983. Growth rate dispersion among ADP crystals formed by primary nucleation. J. Cryst. Growth 61, 215–220.

Gillespie, D.T., 1976. A general method for numerically simulating the stochastic time evolution of coupled chemical reactions. J. Comput. Phys. 22, 403–434.

Gillespie, D.T., 2007. Stochastic simulation of chemical kinetics. Annu. Rev. Phys. Chem. 58, 35–55.

Gilmer, G.H., Bennema, P., 1972. Simulation of crystal growth with surface diffusion. J. Appl. Phys. 43, 1347–1360.

Hu, G., Huang, J., Orkoulas, G., Christofides, P.D., 2009. Investigation of film surface roughness and porosity dependence on lattice size in a porous thin film deposition process. Phys. Rev. E 80, 041122.

Jolliffe, H., Gerogiorgis, D., 2015. Process modeling and simulation for continuous pharmaceutical manufacturing of ibuprofen. Chem. Eng. Res. Des., in press.

Judge, R.A., Forsythe, E.L., Pusey, M.L., 2010. Growth rate dispersion in protein crystal growth. Cryst. Growth Des. 10, 3164–3168.

Kwon, J.S., Nayhouse, M., Christofides, P.D., Orkoulas, G., 2013a. Modeling and control of protein crystal shape and size in batch crystallization. AIChE J. 59, 2317–2327.

Kwon, J.S., Nayhouse, M., Christofides, P.D., Orkoulas, G., 2013b. Modeling and control of shape distribution of protein crystal aggregates. Chem. Eng. Sci. 104, 484–497.

Kwon, J.S., Nayhouse, M., Christofides, P.D., Orkoulas, G., 2014. Protein crystal shape and size control in batch crystallizationcomparing model predictive control with conventional operating policies. Ind. Eng. Chem. Res. 53, 5002–5014.

Kwon, J.S., Nayhouse, M., Orkoulas, G., Ni, D., Christofides, P.D., 2015. A method for handling batch-to-batch parametric drift using moving horizon estimation: application to run-to-run MPC of batch crystallization. Chem. Eng. Sci. 127, 210–219.

Larson, M.A., White, E.T., Ramanarayanan, K.A., Berglund, K.A., 1985. Growth rate dispersion in MSMPR crystallizers. AIChE J. 31, 90–94.

Lovette, M.A., Browning, A.R., Griffin, D.W., Sizemore, J.P., Snyder, R.C., Doherty, M. F., 2008. Crystal shape engineering. Ind. Eng. Chem. Res. 47, 8912–9833.

Nguyen, T.T.H., Hammond, R.B., Marziano, I., Nichols, G., 2014. Precision measurement of the growth rate and mechanism of ibuprofen 001 and 011 as a function of crystallization environment. Cryst. Eng. Commun. 16, 4568–4586.

ÓMeadhra, R., van Rosmalen, G.M., 1996. Modelling of the growth of ammonium sulphate crystals in a DTB crystallizer. Chem. Eng. Sci. 51, 3919–3929.

Randolph, A.D., White, E.T., 1977. Modeling size dispersion in the prediction of crystal-size distribution. Chem. Eng. Sci. 32, 1067–1076.

Rasenack, N., Müller, B.W., 2002. Ibuprofen crystals with optimized properties. Int. J. Pharm. 244, 45–57.

Rashid, A., White, E.T., Howes, T., Litster, J.D., Marziano, I., 2008. Racemic ibuprofen solubility in ethanol and aqueous ethanolic mixtures. In: Proceedings of Chemica 2008, Newcastle, Australia, pp. 1393–1401.

Rashid, A., White, E.T., Howes, T., Litster, J.D., Marziano, I., 2011. Crystallization kinetics of ibuprofen from ethanol and aqueous ethanol. Chem. Eng. Trans. 24, 631–636.

Rashid, A., White, E.T., Howes, T., Litster, J.D., Marziano, I., 2012. Growth rates of ibuprofen crystals grown from ethanol and aqueous ethanol. Chem. Eng. Res. Des. 90, 158–161.

Rasoulian, S., Ricardez-Sandoval, L., 2014. Uncertainty analysis and robust optimization of multiscale process systems with application to epitaxial thin film growth. Chem. Eng. Sci. 116, 590–600.

Rasoulian, S., Ricardez-Sandoval, L., 2015. A robust nonlinear model predictive controller for a multiscale thin film deposition process. Chem. Eng. Sci., in press.

Rathinam, M., Petzold, L.R., Cao, Y., Gillespie, D.T., 2003. Stiffness in stochastic chemically reacting systems: the implicit tau-leaping method. J. Chem. Phys. 119, 12784–12794.

Reese, J.S., Raimondeau, S., Vlachos, D.G., 2001. Monte carlo algorithms for complex surface reaction mechanisms: efficiency and accuracy. J. Comput. Phys. 173, 302–321.

Ricardez-Sandoval, L., 2011. Current challenges in the design and control of multiscale systems. Can. J. Chem. Eng. 89, 1324–1341.

Rohl, A.L., 2003. Computer prediction of crystal morphology. Curr. Opin. Solid State Mater. Sci. 7, 21–26.

Rusli, I.T., Larson, M.A., Garside, J., 1980. Initial growth of secondary nuclei produced by contact nucleation. AIChE Symp. Ser. 76, 52–58.

Shankland, N., Florence, A.J., Cox, P.J., Sheen, D.B., Love., S.W., Stewart, N.S., Wilson, C.C., 1996. Crystal morphology of ibuprofen predicted from single-crystal pulsed neutron diffraction data. Chem. Commun., 855–856.

Shankland, N., Wilson, C., Florence, A.J., Cox, P., 1997. Refinement of ibuprofen at 100K by single-crystal pulsed neutron diffraction. Acta Crystallogr. 53, 951–954.

Shi, D., El-Farra, N.H., Li, M., Mhaskar, P., Christofides, P.D., 2006. Predictive control of particle size distribution in particulate processes. Chem. Eng. Sci. 61, 268–281.

Shi, D., Mhaskar, P., El-Farra, N.H., Christofides, P.D., 2005. Predictive control of crystal size distribution in protein crystallization. Nanotechnology 16, S562–S574.

Snyder, M.A., Chatterjee, A., Vlachos, D.G., 2005. Net-event kinetic Monte Carlo for overcoming stiffness in spatially homogeneous and distributed systems. Comput. Chem. Eng. 29, 701–712.

Vlachos, D.G., 2005. A review of multiscale analysis examples from systems biology, materials engineering, and other fluid-surface interacting systems. Adv. Chem. Eng. 30, 1–61.

Weinan, E., Engquist, B., Huang, Z., 2003. Heterogeneous multiscale method: a general methodology for multiscale modeling. Phys. Rev. B 67, 092101.

Zacher, U., Mersmann, A., 1995. The influence of internal crystal perfection on growth rate dispersion in a continuous suspension crystallizer. J. Cryst. Growth 147, 172–180.